Wave packet spreading and localization in electron-nuclear scattering

Paul E. Grabowski, Andreas Markmann, Igor V. Morozov, Ilya A. Valuev, Christopher A. Fichtl, David F. Richards, Victor S. Batista, Frank R. Graziani, and Michael S. Murillo

Phys. Rev. E **87**, 063104 — Published 10 June 2013

DOI: 10.1103/PhysRevE.87.063104

Wave packet spreading and localization in electron-nuclear scattering

Paul E. Grabowski,[1,*] Andreas Markmann,[2,†] Igor V. Morozov,[3]
Ilya A. Valuev,[3] Christopher A. Fichtl,[1] David F. Richards,[4]
Victor S. Batista,[2] Frank R. Graziani,[4] and Michael S. Murillo[1]

[1] *Computational Physics and Methods Group,*
Los Alamos National Laboratory, Los Alamos, NM 87545, USA
[2] *Department of Chemistry, Yale University, New Haven, CT 06520-8107*
[3] *Joint Institute for High Temperatures of RAS,*
Izhorskaya, 13, Build. 2, Moskow 125412, Russia
[4] *Lawrence Livermore National Laboratory, Livermore, CA 94550*

Abstract

The wave packet molecular dynamics (WPMD) method provides a variational approximation to the solution of the time-dependent Schrödinger equation. Its application in the field of high-temperature dense plasmas has yielded diverging electron localization (spreading), which results in diminishing electron-nuclear interactions. Electron spreading has previously been ascribed to a shortcoming of the WPMD method and has been counteracted by various heuristic additions to the models used. We employ more accurate methods to determine if spreading really occurs and how WPMD can be improved. A scattering process involving a single dynamic electron interacting with a periodic array of statically screened protons is used as a model problem for the comparison. We compare the numerically exact split operator Fourier transform (SOFT) method, the Wigner trajectory method (WTM), and the time-dependent variational principle (TDVP). Within the framework of the TDVP, we use the standard variational form of WPMD, the single Gaussian wave packet (WP). We then generalize this form to include multiple Gaussians for the single electron as in the split WP propagation method. Wave packet spreading is predicted by all methods, so it is not the source of the unphysical electron uniformity of WPMD at high temperatures. Instead, the Gaussian WP's inability to correctly reproduce breakup of the electron's probability density into localized density near the protons is responsible for the deviation from more accurate predictions. Extensions of WPMD must include a mechanism for breakup to occur in order to yield dynamics that lead to accurate electron densities.

* Joint first author: grabowski@lanl.gov

† Joint first author: andreas.markmann@yale.edu

I. INTRODUCTION

There has been extensive work on dense plasmas, with applications ranging from inertial confinement fusion [1], Z-pinch experiments [2], X-ray Thompson scattering [3–5], and exploding wire experiments [6, 7] to describing the astrophysics of white dwarfs [8] and the interiors of giant planets [9–11]. Many of these systems feature strongly non-equilibrium evolution. Dynamical simulation at the particle level is desirable to accurately model the evolution of non-equilibrium plasmas and study energy exchange between electrons, ions, and radiation because of the importance of collisional processes at high densities.

We are interested in calculating transport and collisional properties of dense plasmas. Molecular dynamics (MD), in which particles' positions and velocities evolve classically given an inter-particle force, is a many-body method which includes numerically exact classical collisions. However, in dense plasmas degeneracy and quantum diffraction can be important for describing the electrons. Furthermore, classical electrons and ions may collapse into the singular Coulomb wells via many-body interactions. The potential energy is converted to an arbitrarily large amount of kinetic energy, given to nearby particles, unphysically heating the system. The classical approximation for the ion dynamics is still usually valid for the relatively heavy ions, so we focus on methods that employ MD for the ions and treat electrons quantum mechanically.

Ideally, we want to calculate a numerically converged solution to the many-body time-dependent Schrödinger equation (TDSE) for the electron wave function in the external potential due to the ions. Tens or a few hundred degrees of freedom can be evolved with the efficient multi-configuration time-dependent Hartree (MCTDH) method [12, 13]. Despite making significant progress in reducing the computational effort for many-body quantum problems, MCTDH still scales exponentially with the number of degrees of freedom and cannot handle the system sizes needed to represent temperature and density gradients commonly found in the dense plasmas listed above. The use of quantum statistical potentials (QSPs) [14, 15] within MD yields quasi-dynamics, but requires a temperature which explicitly appears in the potential. Properties of quasi-equilibrium problems, such as temperature relaxation, may be valid [16], but fully non-equilibrium dynamics cannot be trusted.

The wave packet molecular dynamics (WPMD) method [17, 18] is an alternative we wished to validate or invalidate. Each electron's wave function is usually modeled by an

isotropic (spherical) Gaussian wave packet (WP), whose parameters obey equations of motion derived from the time-dependent variational principle (TDVP) while ions are usually treated classically with standard MD. Electron interactions with other particles depend explicitly on electron states and not on global statistical properties such as temperature. This method is capable of simulating non-equilibrium dynamics and gives a well-defined approximation to the many-body TDSE, while also being easy to implement in an MD code. The Gaussian ansatz was first used to simulate scattering between simple atoms [17]. It was later adopted by the nuclear physics community [18, 19] to understand nuclear structure and reactions. Klakow, Toepffer, and Reinhard [20, 21] were the first to apply WPMD to plasmas. The Gaussian ansatz seemed reasonable because at high temperatures, electrons were expected to approximate classical behavior [20]. However, electrons as simulated by WPMD feature divergent width parameters leading to wave packet spreading [22–29]. Electrons then overlap all ions, with no mechanism to localize near nuclei, producing a nearly constant electron background at large times.

Knaup, Reinhard, and Toepffer [22] introduced an *ad hoc* fix to wavepacket spreading by adding a harmonic constraint to the wave packet (WP) width. Later, Ebeling and coworkers [28] derived this term from the TDVP by imposing a position-dependent phase factor with constant nonzero coefficient to the variational ansatz. These approaches include an arbitrary fixed parameter that determines the width of the harmonic well acting on the WP width. Morozov and Valuev [29] showed that by varying the constraint, they could obtain any value of the dynamical collision rate; including the constraint makes WPMD an empirical model.

Wave packet spreading is reduced by antisymmetrization of the wave function, allowing simulations at slightly higher than the Fermi temperature [30]. Several flavors of WPMD exist to take into account Fermi statistics. Full antisymmetrization requires order N^4 [19] operations. A less demanding approach is pairwise antisymmetrization [20–23, 31] or only antisymmetrizing with respect to the kinetic energy [25–27, 32, 33]. Alternatively, in the electron force field (eFF) method, a Pauli potential with empirical parameters fit to highly accurate molecular properties is added [30, 34, 35]. With eFF, improved agreement between simulations and recent Z-pinch [2] and high explosive [36] Hugoniot measurements is obtained. The impact of multiparticle properties such as antisymmetrization on wave packet spreading is not studied in this article.

In order to decide whether spreading is physical, we study a scattering process involving

a single dynamic electron interacting with a realistic static dense plasma charge density, described in Sec. III. This simple system was chosen in order to allow simulation methods employing different degrees of approximation, thereby offering a range of physical insights. With this test problem the Gaussian ansatz of WPMD is directly compared to more accurate methods.

II. METHODS

For many-particle systems, numerically converged quantum dynamics are computationally infeasible, so approximate methods are needed. Here, we present several methods applied to a single electron problem. Generalization to many electron systems is complicated by the enforcement of a totally antisymmetric wave function and the additional computational effort. We outline several approximations to the TDSE, including the TDVP in Sec. II A, with both the single Gaussian WP and split WP ansatzes, and the Wigner trajectory method (WTM) in Sec. II B. For single electron scattering, we can afford to quantify the success of these approximate methods by comparison with quantum dynamics obtained from the split operator Fourier transform (SOFT) method (Sec. II C). We also present the well known non-interacting WP solution in Sec. II D so that the impact of scattering can be quantified.

In all cases, the initial state is an isotropic (spherical) Gaussian with given initial position and momentum vectors and given scalar width. All quantities are understood to be in atomic units unless otherwise noted, i.e. $\hbar = 1$, length is measured in Bohr, $a_0 \approx 0.52918$ Å, and energy in Hartree, $E_\mathrm{h} \approx 27.211$ eV.

A. The time-dependent variational principle (TDVP)

The TDVP leads to a rigorous approximation of the TDSE with a given variational ansatz. With this method the residual of the TDSE is minimized over a given subspace of states $|\psi\rangle$, so that

$$\delta \int_{t_i}^{t_f} \left\langle \psi \left| \mathrm{i}\frac{\partial}{\partial t} - \hat{H} \right| \psi \right\rangle dt = 0, \tag{1}$$

where t_i and t_f are the initial and final times of the integration, and $\hat{H}$ is the Hamiltonian. If the state $|\psi\rangle$ is allowed to vary throughout a Hilbert space that includes the solution, the TDSE will be exactly solved. Otherwise, the error in the state grows linearly with time over short times [18].

A variational state $|\boldsymbol{q}\rangle$ can be parametrized by a vector of complex time-dependent variational parameters,

$$\mathbf{q} = \{q_1, q_2, \ldots, q_{N_v}\}. \tag{2}$$

The variational parameters follow the equations of motion [18]:

$$\mathrm{i}\boldsymbol{N}\dot{\mathbf{q}} = \frac{\partial\langle\hat{H}\rangle}{\partial\mathbf{q}^*}, \quad -\mathrm{i}\boldsymbol{N}\dot{\mathbf{q}}^* = \frac{\partial\langle\hat{H}\rangle}{\partial\mathbf{q}}, \tag{3}$$

where $\langle\hat{O}\rangle = \langle\psi|\hat{O}|\psi\rangle$ and * denotes the complex conjugate. The Hermitian norm matrix is defined by [18]:

$$N_{ab} = \frac{\partial}{\partial q_a^*}\frac{\partial}{\partial q_b}\ln\langle\mathbf{q}|\mathbf{q}\rangle. \tag{4}$$

Note, Eqs. (3) are time reversed forms of each other; so models derived from the TDVP preserve time reversal symmetry. For special choices of the variational form and parameters, the matrix $\boldsymbol{N}$ reduces to a trivially-inverted matrix and canonical positions and momenta can be defined that make the equations of motion have a Hamilton form in N_v dimensions (see for example Ref. [37]):

$$\dot{\boldsymbol{\rho}} = \frac{\partial\langle\hat{H}\rangle}{\partial\boldsymbol{\pi}}, \qquad \dot{\boldsymbol{\pi}} = -\frac{\partial\langle\hat{H}\rangle}{\partial\boldsymbol{\rho}}. \tag{5}$$

In spite of the persuasiveness of this form, it has to be noted that $\boldsymbol{\rho}$ and $\boldsymbol{\pi}$ are variational parameters inextricably tied to a particular variational wave function form that should not be mistaken for classical positions and momenta. Using the TDVP with a small number of parameters requires physical intuition as to the form of the wave function. It must be flexible enough to give reasonable observables as well as numerically convenient and capable of representing the desired initial state.

1. Gaussian wave packet

The Gaussian WP wave function is parameterized as

$$\varphi_G(\boldsymbol{x}, t) = \left(\frac{3}{2\pi\sigma^2}\right)^{3/4} e^{-\gamma|\boldsymbol{x}-\boldsymbol{r}|^2 + i\boldsymbol{p}\cdot(\boldsymbol{x}-\boldsymbol{r})} \tag{6}$$

where

$$\gamma = \frac{3}{4\sigma^2} + \frac{\mathrm{i}p_\sigma}{2\sigma}. \tag{7}$$

This ansatz depends on 8 real time-dependent variational parameters, $(\boldsymbol{r}, \sigma, \boldsymbol{p}, p_\sigma)$, representing position and momentum vectors as well as scalar width and conjugate width momentum of the isotropic (spherical) Gaussian, respectively. A wave function which is initially a Gaussian will not remain a Gaussian at all times unless the potential has zero third and higher derivatives. However the Gaussian ansatz forces this to always be true, obtaining the Gaussian closest to the exact solution at short times.

Equations (1) and (6) lead to the equations of motion

$$\dot{\boldsymbol{r}} = \frac{\partial \langle \hat{H} \rangle}{\partial \boldsymbol{p}}, \qquad \dot{\boldsymbol{p}} = -\frac{\partial \langle \hat{H} \rangle}{\partial \boldsymbol{r}}, \tag{8}$$

$$\dot{\sigma} = \frac{\partial \langle \hat{H} \rangle}{\partial p_\sigma}, \qquad \dot{p}_\sigma = -\frac{\partial \langle \hat{H} \rangle}{\partial \sigma}, \tag{9}$$

which have the same form as the classical Hamilton equations except that an extra degree of freedom has been added (σ) and the classical Hamiltonian is replaced by the quantum expectation value of the Hamilton operator, leading to significantly adjusted dynamics.

2. Split wave packet

A generalization of the Gaussian WP is the split WP [38], which represents a single electron wave function by M Gaussians with mixing coefficients c_α:

$$\varphi_s(\boldsymbol{x}, t) = n^{-1/2} \sum_{\alpha=1}^{M} c_\alpha \varphi_\alpha(\boldsymbol{x}, t), \tag{10}$$

where

$$n = \sum_{\alpha,\beta} c_\alpha^* c_\beta \int \varphi_\alpha^* \varphi_\beta d\boldsymbol{x} \tag{11}$$

is the normalizing factor for φ_s. Each WP (φ_α) has the same form as Eq. (6), where the variational parameters ($\boldsymbol{r}$, $\boldsymbol{p}$, σ, and p_σ) take on different values and evolve independently for each WP.

The term "split" in the name of the method originates from the possibility of using this variational form [Eq. (10)] for the simulation of wave function splitting into multiple branches. Incorporating initially unpopulated Gaussians (having vanishing weights) into a

basis set creates a solution subspace for quantum branching. The initial parameters for these auxiliary Gaussians may often be anticipated from the physical conditions, thus keeping the dimension of the basis set small. Although M may be changed dynamically, in the present work we fix M and place the auxiliary basis functions at the minima of the potential.

The time-dependent complex coefficients $c_\alpha(t)$ together with the M sets of standard WP parameters $\{\boldsymbol{r}_\alpha(t), \sigma_\alpha(t), \boldsymbol{p}_\alpha(t), p_{\sigma_\alpha}(t)\}$ constitute a set of dynamic variables for a moving electron. Due to the normalization condition and the free choice of a constant phase, there are $10M-2$ independent parameters for the single electron, consistent with the 8 parameters of WPMD for $M = 1$.

In the Gaussian basis the interaction matrix elements of single-electron operators ($\hat{T}$ and $\hat{V}$) are proportional to the corresponding WP overlaps $o_{\alpha\beta} = \int \varphi_\alpha^* \varphi_\beta d\boldsymbol{x}$:

$$\langle\varphi_\alpha|\hat{T}|\varphi_\beta\rangle = \frac{1}{2}\boldsymbol{\nabla}_{\boldsymbol{r}_\alpha} \cdot \boldsymbol{\nabla}_{\boldsymbol{r}_\beta} o_{\alpha\beta}, \tag{12}$$

$$\langle\varphi_\alpha|\hat{V}|\varphi_\beta\rangle = V_{\alpha\beta} o_{\alpha\beta}, \tag{13}$$

where $V_{\alpha\beta}$ can be calculated analytically by integration for many simple forms of $\hat{V}$. The variational total energy of the split WP model is:

$$\langle\hat{H}\rangle = n^{-1} \sum_{\alpha,\beta} \left(\frac{1}{2}\boldsymbol{\nabla}_{\boldsymbol{r}_\alpha} \cdot \boldsymbol{\nabla}_{\boldsymbol{r}_\beta} + V_{\alpha\beta} \right) (c_\alpha^* o_{\alpha\beta} c_\beta). \tag{14}$$

The norm matrix needs to be evaluated and inverted at every time step for $M > 1$. The overcompleteness of the Gaussian basis may lead to a degenerate norm matrix, adding computational burden to the split WP algorithm, especially since it is often nearly singular due to significant overlap between Gaussians. Large time derivatives of the variational parameters may occur, forcing reduction of the time step. Variable time stepping needs to be employed to preserve the total energy within a given accuracy (of the order of 10^{-5} Hartree).

The initial state of the split WP should be equivalent to the Gaussian WP form, requiring only the first of the WPs to have non-zero weight. However, populating only a single Gaussian leads to a singular norm matrix, so the initial state is perturbed by setting $c_\alpha(0) = 0.001$ for $\alpha > 1$ and correcting c_1 accordingly. The other initial values for the time-dependent variational parameters of the auxiliary WPs are determined by choosing time-independent variational minima of single Gaussian WPs, as these minima correspond to the peaks of electron density once that area of space is populated by the electron. By ordering the

minima by their overlap with the initial Gaussian, a small number of Gaussian basis functions additional to the initial state can be selected.

B. Wigner trajectory method (WTM)

An alternative, but equivalent, formulation of the TDSE that yields to both different approximations and complementary insights is the WTM [39–41]. We start with the six-dimensional Wigner transform of the wave function [42]

$$f_W(\boldsymbol{x},\boldsymbol{p},t) = \int \frac{\mathrm{d}\boldsymbol{s}\,\mathrm{e}^{\mathrm{i}\boldsymbol{p}\cdot\boldsymbol{s}}}{(2\pi)^3}\varphi^*\left(\boldsymbol{x}+\frac{\hbar\boldsymbol{s}}{2},t\right)\varphi\left(\boldsymbol{x}-\frac{\hbar\boldsymbol{s}}{2},t\right), \tag{15}$$

which obeys the time-dependent Wigner equation

$$\left(\frac{\partial}{\partial t}+\frac{\boldsymbol{p}}{m}\cdot\boldsymbol{\nabla}_{\boldsymbol{x}}+\hat{O}_{QM}\right)f_W(\boldsymbol{x},\boldsymbol{p},t)=0, \tag{16}$$

where

$$\hat{O}_{QM}f_W(\boldsymbol{x},\boldsymbol{p},t) = \int d\boldsymbol{p}' V_W(\boldsymbol{x},\boldsymbol{p}-\boldsymbol{p}')f_W(\boldsymbol{x},\boldsymbol{p}',t), \tag{17}$$

$$V_W(\boldsymbol{x},\boldsymbol{p}) = \int \frac{d\boldsymbol{s}\,\boldsymbol{e}^{-\mathrm{i}\boldsymbol{p}\cdot\boldsymbol{s}}}{\mathrm{i}(2\pi)^3\hbar}\left[V\left(\boldsymbol{x}-\frac{\hbar\boldsymbol{s}}{2}\right)-V\left(\boldsymbol{x}+\frac{\hbar\boldsymbol{s}}{2}\right)\right], \tag{18}$$

and

$$V(\boldsymbol{x}) = \langle\boldsymbol{x}|\hat{V}|\boldsymbol{x}\rangle. \tag{19}$$

These equations encode the non-locality of quantum mechanics; a quantum particle interacts with the potential throughout all of space. We wish to explore how important non-locality is, so we remove the non-locality by assuming V is slowly varying and Taylor expand V about $\boldsymbol{s}=\boldsymbol{0}$, which yields

$$\begin{aligned}\hat{O}_{QM}f_W(\boldsymbol{x},\boldsymbol{p},t) = &-\frac{\hbar^0}{2^0 1!}\partial_i^{\boldsymbol{x}}V(\boldsymbol{x})\partial_i^{\boldsymbol{p}}f_W(\boldsymbol{x},\boldsymbol{p})\\ &+\frac{\hbar^2}{2^2 3!}\partial_{ijk}^{\boldsymbol{x}}V(\boldsymbol{x})\partial_{ijk}^{\boldsymbol{p}}f_W(\boldsymbol{x},\boldsymbol{p})-\ldots,\end{aligned} \tag{20}$$

where repeated indices imply a summation, $\partial_i^{\boldsymbol{v}}$ is the partial derivative with respect to the ith part of $\boldsymbol{v}$, and $\partial_{ijk}^{\boldsymbol{v}} = \partial_i^{\boldsymbol{v}}\partial_j^{\boldsymbol{v}}\partial_k^{\boldsymbol{v}}$. Here we will only keep the first term on the right hand side,

$$\hat{O}_{QM}f_W(\boldsymbol{x},\boldsymbol{p},t) \approx \boldsymbol{F}\cdot\boldsymbol{\nabla}_{\boldsymbol{p}}f_W(\boldsymbol{x},\boldsymbol{p},t), \tag{21}$$

where

$$\boldsymbol{F} = -\boldsymbol{\nabla}_{\boldsymbol{x}} V(\boldsymbol{x}), \tag{22}$$

which leaves us with

$$\left(\frac{\partial}{\partial t} + \frac{\boldsymbol{p}}{m} \cdot \boldsymbol{\nabla}_{\boldsymbol{x}} + \boldsymbol{F} \cdot \boldsymbol{\nabla}_{\boldsymbol{p}}\right) f_W(\boldsymbol{x}, \boldsymbol{p}, t) = 0. \tag{23}$$

This is the Thomas-Fermi (long wavelength) limit. One can also think of Eq. (20) as an $\hbar$ expansion. In this sense Eq. (21) is the classical limit. However, we stress that $\hbar$ has not been set to zero everywhere; the initial distribution satisfies the Heisenberg uncertainty principle for the physical value of $\hbar$ and f_W should be thought of as an approximate quantum state. Equation (23) has the exact solution

$$f_W(\boldsymbol{x}, \boldsymbol{p}, t) = f_W(\boldsymbol{x}(t), \boldsymbol{p}(t), 0), \tag{24}$$

where

$$\dot{\boldsymbol{x}}(t) = \boldsymbol{p}(t) \quad \text{and} \quad \dot{\boldsymbol{p}}(t) = \boldsymbol{F}(\boldsymbol{x}(t)), \tag{25}$$

from the method of characteristics [39]. For a Gaussian initial state, the Wigner transform is positive definite, as it is a Gaussian in phase space. It can then be used to sample an initial phase space distribution of point masses. The characteristic trajectories of the Wigner distribution are obtained by classical Velocity-Verlet integration [43] of Eq. (23) [15, 44]. The WTM results illuminate whether the uncertainty in the position and momentum of the wave function is the dominant quantum effect in the process studied, since other quantum effects such as interference and tunneling are missing from WTM.

A complication arises when an electron experiences a close encounter with an ion - the gradient of the potential then becomes divergent. Here, we simply use a sufficiently small time step so that the final density is converged. We also note that the expansion, Eq. (20) is invalid near the singularities. The convergence radius of the Taylor expansion extends only to the singularity of the nearest neighbor nuclear interaction potential. So one should not try too hard to numerically solve Eq. (23) in the vicinity of the ions because the model is incorrect there. We rely on the fact that these regions are small in phase space and so do not have too large an effect on most parts of the density.

C. The split operator Fourier transform (SOFT) method

It is useful to have a method that can be used as a reference to compare against the approximate models described above. This reference can also be used to inspire improvements to the other models. For a single electron problem, the Schrödinger equation is:

$$\mathrm{i}\frac{\partial}{\partial t}\varphi\left(\boldsymbol{x},t\right)=\left(\hat{T}+\hat{V}\right)\varphi\left(\boldsymbol{x},t\right), \tag{26}$$

where $\hat{T}$ and $\hat{V}$ are the kinetic and potential energy operators, respectively. Equation (26) is solved by repeated application of the propagation operator for a time step Δt, approximated by the split operator [45–49]

$$U\left(t,t+\Delta t\right)=\mathrm{e}^{-\mathrm{i}\hat{V}\Delta t/2}\mathrm{e}^{-\mathrm{i}\hat{T}\Delta t}\mathrm{e}^{-\mathrm{i}\hat{V}\Delta t/2}+\mathcal{O}[\Delta t^{3}]. \tag{27}$$

The SOFT method takes advantage of this factorization by applying the first and third operator in position space and the second in momentum space because these operators are diagonal in those spaces. The basis change from coordinate space to momentum space and vice versa is realized by forward and backward fast Fourier transforms on the equidistant grid.

The complex wave function $\varphi\left(\boldsymbol{x},t\right)$ at time t is represented on a grid

$$x_{\alpha k}=x_{\alpha 0}+k\cdot\Delta x,\ k=1,\ldots,128,$$

where α enumerates the three Cartesian directions, $x_{10}=x_{20}=x_{30}=-L/2$, $\Delta x=L/128$, small enough to correctly represent the momenta of the wave function at the energy range given, and L is the length of the cubic box. Because the error in the propagator [Eq. (27)] is proportional to commutators involving the potential energy, the required time step is controlled by the size of gradients in the potential on the grid. We minimize this effect by ensuring that no ion is too close to the grid points.

D. Non-interacting wave packet

It is instructive to compare the motion of an electron with that of a non-interacting electron, *i.e.* an electron with the same initial conditions moving through a vacuum. The exact non-interacting Gaussian solution at time t is

$$\varphi_{n}(\boldsymbol{x},t)=\varphi_{G}(\boldsymbol{x},t)e^{\mathrm{i}\theta} \tag{28}$$

with

$$\theta = (t - t_0)\frac{p_0^2}{2} - \frac{3}{2}\tan^{-1}\left(\frac{3(t-t_0)}{2\sigma_0^2}\right) \tag{29}$$

$$\boldsymbol{r} = \boldsymbol{p}_0(t - t_0) + \boldsymbol{r}_0 \tag{30}$$

$$\boldsymbol{p} = \boldsymbol{p}_0 \tag{31}$$

$$\sigma = \sigma_0\sqrt{1 + \frac{9(t-t_0)^2}{4\sigma_0^4}} \tag{32}$$

$$p_\sigma = \frac{9(t-t_0)}{4\sigma\sigma_0^2}, \tag{33}$$

where the minimum uncertainty WP is assumed at the initial time $t = t_0$ and values of the variational parameters at this time are marked by the subscript 0. The extra phase factor, θ, compared to the Gaussian WP makes no difference in the density. Free particle dynamics always lead to a spreading WP. A potential may act on a WP by localizing or spreading it. By directly comparing with the non-interacting WP solution, we will examine which of the two processes is occurring.

III. QUANTUM PINBALL

To compare the methods of Sec. II, single electron dynamics are simulated in a realistic model plasma, given by the following:

1. Ions are fixed at positions derived from a snapshot of a QSP MD simulation equilibrated at $T = 50$ eV and ion number density $n = 10^{24}$ cm^{-3} and then slightly modified as described in Sec. II C . The ions are bare nuclei of charge $Z = 1$.

2. Background electrons are treated implicitly by taking into account screening of the ionic Coulomb potentials by replacing them with Yukawa potentials having a screening length λ of 1Å.[1]

3. An infinite system is approximated by periodic boundary conditions. The number of ions per unit cell is 500.

[1] The Yukawa screening model begins to break down at high densities/low temperatures because the number of electrons per cubic screening length becomes of order or less than unity. In order to correct for this failure, non-linear screening is needed. In the interest of simplicity of the model, we study the failure of the Gaussian ansatz with the Yukawa model. When using each of the methods described in the previous section, we make this approximation, so direct comparisons between them are still valid.

Preliminary tests were presented in Refs. [15, 44] with a finite (non-periodic) smaller cluster of Coulomb potentials; here, the Yukawa potential more realistically models scattering of a recently ionized electron in the bulk of a plasma dominated by fast electrons, for which static screening of the ions is a good approximation. However, none of the methods in Sec. II are inherently limited to static nor short-range potentials, although such changes incur additional costs.

The Hamiltonian operator of the quantum pinball problem is then

$$\hat{H} = \hat{T} + \hat{V}, \tag{34}$$

where

$$\hat{T} = \frac{\hat{\boldsymbol{p}}^2}{2}, \tag{35}$$

$$\langle \boldsymbol{x}|\hat{V}|\boldsymbol{x}\rangle = -\sum_I V_{\text{Yukawa}}\left(|\boldsymbol{R}_I - \boldsymbol{x}|\right), \tag{36}$$

and

$$V_{\text{Yukawa}}(r) = \frac{1}{r}e^{-r/\lambda}. \tag{37}$$

Here, $\hat{\boldsymbol{p}}$ is the momentum operator, $|\boldsymbol{x}\rangle$ is a position eigenstate, $\boldsymbol{R}_I$ are the ion positions, and $\lambda = 1\text{Å}$ is the screening length.

In this section, we emphasize the differences between the Yukawa screened potential and bare Coulomb for the Gaussian ansatz of the TDVP, compare the simulation times and densities of the Gaussian WP propagated with the methods of Sec. II, and quantify localization and breakup.

A. Gaussian wave packet Hamiltonian

With Eqs. (34-37), the expectation value of the Hamiltonian can be explicitly evaluated. Here, we calculate that expectation value for the Gaussian WP so that its dynamics can be directly explained. The derivatives of this expectation value with respect to the variational parameters yield the time derivatives of those parameters according to Eqs. (8) and (9). The kinetic and potential expectation values are

$$\langle \hat{T}\rangle = \frac{p^2}{2} + \frac{p_\sigma^2}{2} + \frac{9}{8\sigma^2}, \tag{38}$$

$$\langle \hat{V}\rangle = \sum_I V_{exp}\left(|\boldsymbol{r} - \boldsymbol{R}_I|, \sigma\right), \tag{39}$$

where

$$V_{exp}\left(r,\sigma\right) = -\frac{1}{2r}e^{\sigma^2/6\lambda^2}\left[V_+(r,\sigma) + V_-(r,\sigma)\right] \tag{40}$$

$$V_\pm\left(r,\sigma\right) = \mathrm{e}^{\pm r/\lambda}\left\{\mathrm{erf}\left[\sqrt{\frac{3}{2}}\left(\frac{r}{\sigma} \pm \frac{\sigma}{3\lambda}\right)\right] \mp 1\right\}. \tag{41}$$

The first term $(p^2/2)$ on the right of Eq. (38) is the translational kinetic energy, while the latter two are due to the uncertainty in the value of the momentum. The first of these, $(p_\sigma^2/2)$, depends on the temporal change of the width in a manner very similar to the translational kinetic energy. A positive (negative) value of p_σ signifies a growing (shrinking) width. If $p_\sigma = 0$, the Gaussian WP is a minimum uncertainty WP. The last term $(9/8\sigma^2)$ produces an infinite energy barrier to having zero width. The physical reason for this term stems from the position-momentum uncertainty principle. A small width implies a large uncertainty in momentum, so the second moment of momentum about $\boldsymbol{p}$ must be large as well. These three terms produce the dynamics of the non-interacting WP, which approximates the dynamics when either $\sigma \ll a_I$ or $\sigma \gg a_I$, where a_I is the ion sphere radius defined by the average space-filling sphere volume per ion at a given number density.

B. Comparison of simulation times

To give a sense of the relative computational effort needed for this single electron problem, we present the simulation times in Tab. I. Because we ran these simulations on different types of computers with differing amounts of parallelization and different programmers, ratios of times should be taken as rough guides of relative computational effort. The Gaussian WP evolution is the fastest. When multiple WPs are employed per electron as in the split WP method, the computational time increases with M for three reasons: there are more parameters to evolve, a matrix equation whose size scales with M and the solution of which is trivial for $M = 1$, must be solved to extract time derivatives of the variational parameters, and the likelihood of the norm matrix becoming nearly singular increases. If the norm matrix is dense, the computational time for the split WP method scales as M^3, otherwise the scaling is M^2. The singular norm matrix events are quasi-random, which is why the $M = 3$ case took the longest. Having an adaptive time step algorithm is important for accurately integrating these events. Both the Gaussian and split WP methods can be parallelized by splitting

Method	CPU time per step	# of steps	CPU time	# of CPUs	Wall clock time
Gaussian WP	13.8 ms	105	1.45 s	11	0.15 s
split WP $M = 2$	984. ms	127	125. s	11	12.1 s
split WP $M = 3$	1.93 s	345	666. s	11	61.5 s
split WP $M = 4$	2.37 s	137	325. s	11	30.7 s
split WP $M = 5$	3.68 s	137	504. s	11	47.4 s
WTM	82.0 s	5×10^5	475. d	480	23.7 hr
SOFT, pot.	N.A.	N.A.	15 hr	1	15 hr
SOFT, dyn.	864. ms	500	7.2 min	1	7.2 min

Table I. Comparison of computation times of the different methods to propagate the 8.8 eV electron for 50 as. The time for the SOFT method is split into the time for calculating the potential at all 128^3 grid points (SOFT, pot.) and the propagation time (SOFT, dyn.).

the work of calculating the expectation value of the potential energy amongst the available processors.

The WTM suffers from having to integrate particle trajectories near Coulomb singularities. We solved this problem with brute force, hence the enormous total computational time of over a year. The algorithm is efficiently parallelized because each particle used to represent the electron's density evolves independently of the others due to the local approximation made to the Wigner equation in Eq. (16). It was much easier to parallelize our algorithm than to make it more efficient. Modifications to improve the algorithm should include changing the algorithm from a fixed time step to an adaptive one, as well as splitting the time propagation into an exact Kepler part and a numerical non-singular part [44]. We expect a speedup of several orders of magnitude from such improvements because our current algorithm used a thousand or more times as many time steps as the other methods, which was fixed by the rare hard collisions between the numerical particles and the ions. Note, neither the Gaussian nor split WP forms resolve the Coulomb singularity, which is one reason they are less computationally expensive.

The computational time for the SOFT method is split between calculating the potential at each grid point, which involves summing the contributions to the potential at all 128^3

grid points due to the 500 protons and each of their 27 nearest images. The large amount of time to calculate these quantities, 15 hours, was why we were forced to fix the protons. The large mass ratio of the proton to the electron makes this approximation a valid one for our purpose of testing electron dynamics. Actually propagating the electron took only a little more than seven minutes. So we were able to save the potential data and quickly rerun with other initial conditions. The potential calculation is easier to parallelize than the time propagation because the latter relies heavily on fast Fourier transforms, which require global information of the wave function at all Fourier grid points. Note, doing the two-electron problem at the same resolution would have required more than a million times greater computational effort. Therefore, we present SOFT only as a reference.

C. Comparison of predicted electron densities and widths

The initial wave function is a single Gaussian, representable by all methods in Sec. II:

$$\varphi(\boldsymbol{x}, t=0) = \left(\frac{3}{2\pi\sigma^2}\right)^{3/4} \exp\left(-\frac{3}{4\sigma^2}|\boldsymbol{x}|^2 + i\boldsymbol{p}\cdot\boldsymbol{x}\right), \tag{42}$$

where $\sigma = \sqrt{3}\,\text{Å}$, $\boldsymbol{p}$ is in the $x-$direction, and we have chosen its magnitude by setting $p^2/2m = 8.8$, 62.5, 250, and 1000 eV. The first value was used for all methods, while the latter three were only done with SOFT, Gaussian WP, and the non-interacting WP. The last three values match those of Ref. [15]. The initial density integrated over the z-coordinate is shown in Fig. 1. The initial wave function was evolved in three dimensions using SOFT, Gaussian WP, split WP ($M = 5$), and WTM, producing the densities shown in Figs. 2 and 3 at times when the non-interacting WP is displaced 0.99 Å. The non-interacting electron case ($V \equiv 0$) is also shown for comparison. There are two comparisons to make for each approximate method. We compare to the SOFT result to test for accuracy, and we compare to the non-interacting WP result to see how the potential affects their dynamics.

At high impact energies, the Gaussian WP agrees very well with the SOFT and non-interacting WP results, as the wave function remains approximately spherical while it is displaced by about 1 Å. At lower impact energies, the non-interacting WP has a significantly smaller width than the Gaussian WP, so the net effect of the potential on a WP this size is to make it spread. Attractive Coulomb potentials always slow down the growth of σ or

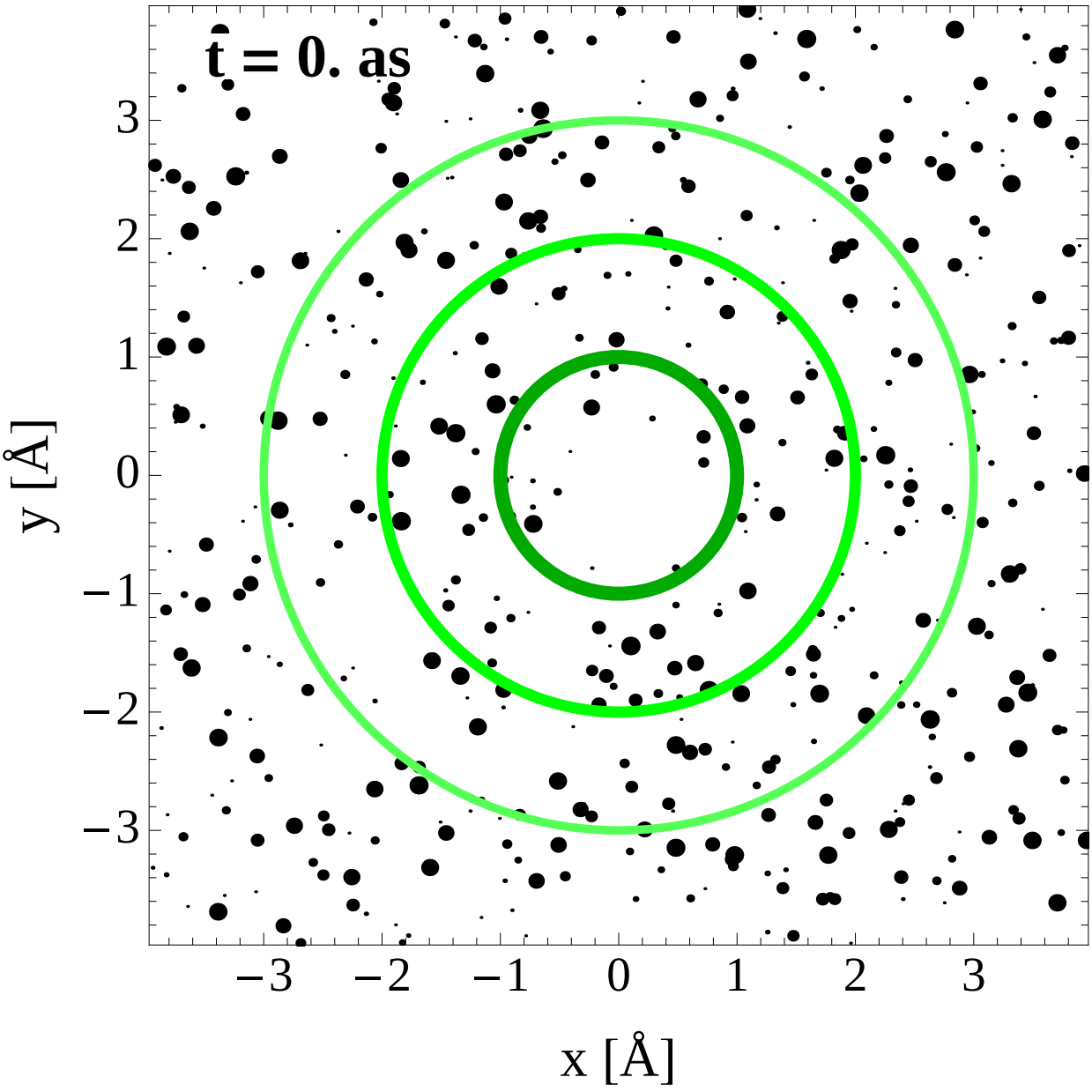

Figure 1. (Color online) Probability density isocontours of the initial state integrated over the z coordinate. The three contours represent 60.7% (dark), 13.5% (medium), and 1.1% (light) of the maximum density. The black dots represent fixed protons, with the larger dots being protons closer to the $z = 0$ plane.

accelerate its reduction, as can be seen by the $\lambda \to \infty$ limit of V_{exp} [see Eq. (40)]:

$$\lim_{\lambda\to\infty} V_{exp}(r,\sigma) = -\frac{1}{r}\mathrm{erf}\left(\sqrt{\frac{3}{2}}\frac{r}{\sigma}\right), \tag{43}$$

while repulsive Coulomb potentials do the opposite. The attractive Yukawa screened poten-

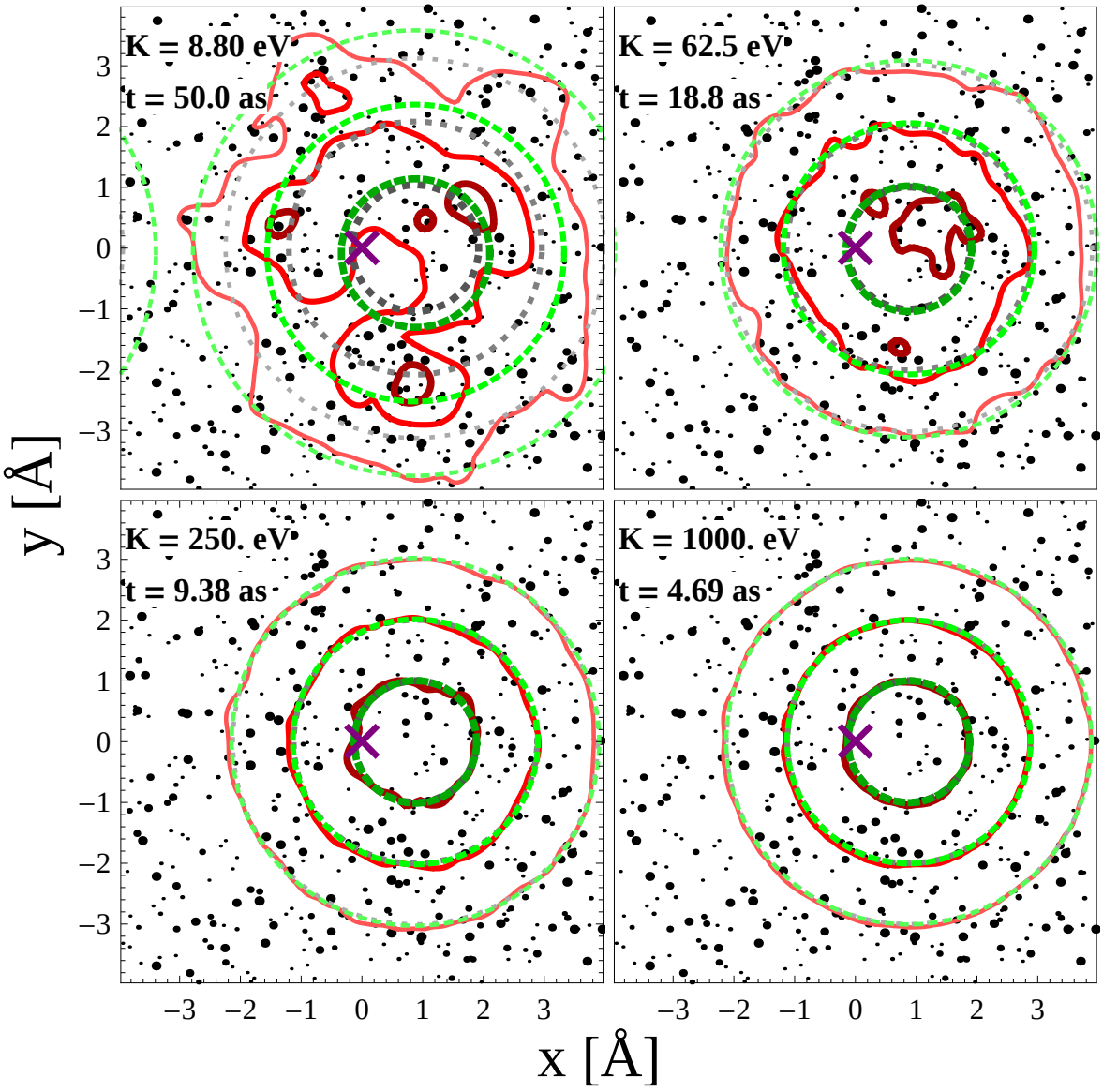

Figure 2. (Color online) Propagated electron densities after the center of the non-interacting WP has moved 0.99 Å for four initial translational kinetic energies, $K = \langle \hat{p} \rangle^2 / 2m$, showing the predictions of SOFT (solid red), Gaussian WP (long-dashed green), and the non-interacting electron (short-dashed gray). Note, the higher energy cases are shown at earlier times so that all cases have roughly the same displacement. The purple × indicates where the center of the WP was initially, at $t = 0$. The Gaussian WP gives reasonable agreement with SOFT at high kinetic energies, while at lower energies, the SOFT density shows localization which cannot be represented with a single Gaussian. In comparison to the non-interacting electron, the pinball potential delocalizes the electron density, which can be seen most easily at low energies.

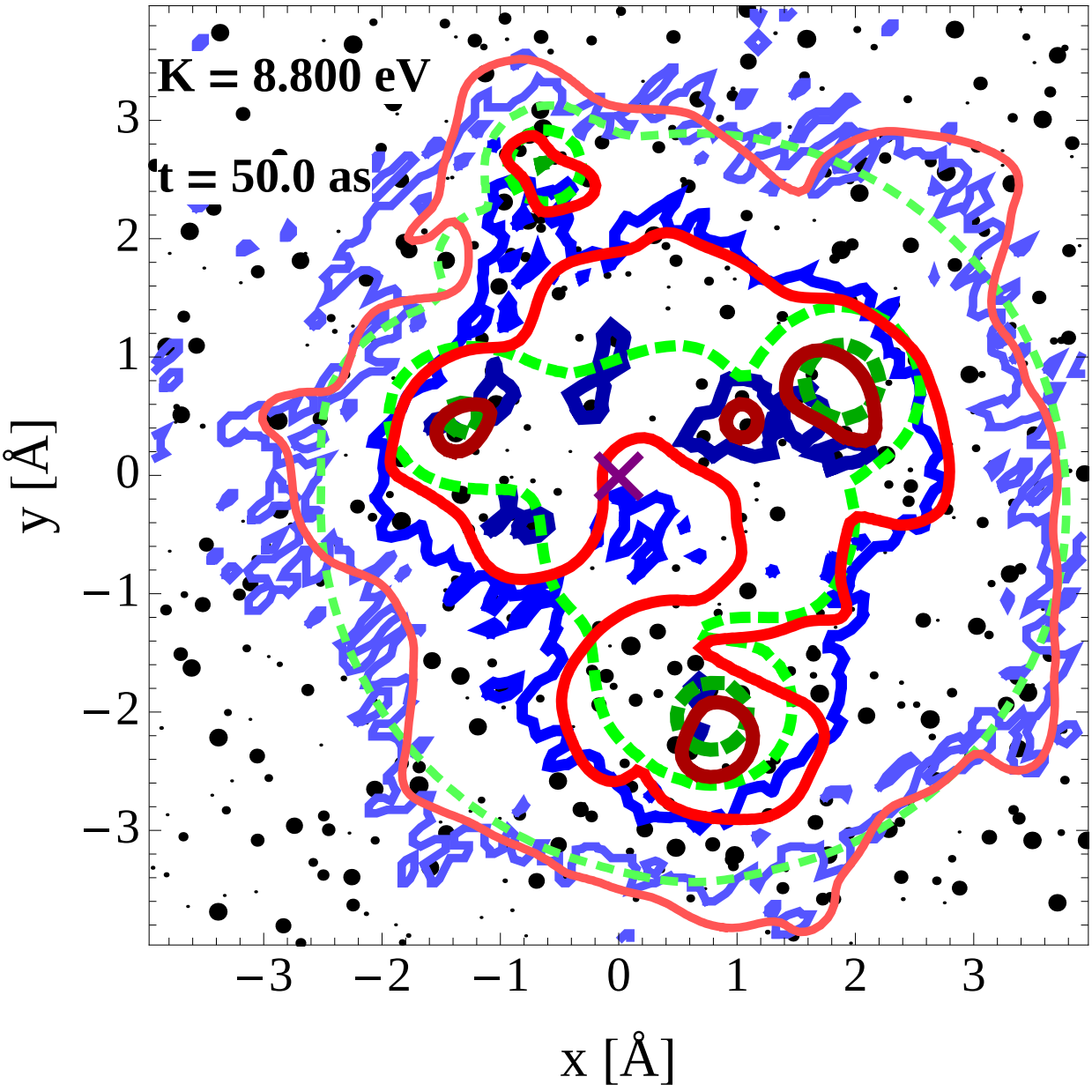

Figure 3. (Color online) Same as Fig. 2 except at only 8.8 eV and densities as predicted by SOFT (solid red), split WP with $M = 5$ (dashed green), and WTM (noisy blue). It can be seen that the more flexible approximate methods split WP and WTM are capable of reproducing wave packet break-up and considerably improve agreement with the SOFT density.

tial can do both because it represents the effects of both the bare nucleus and the electrons around it. The σ-dependence of the potential energy of a Gaussian centered away from a single Yukawa well has a minimum at a positive value (Fig. 4). So the Gaussian WPs will have a tendency to grow until a significant portion of their densities overlap neighboring

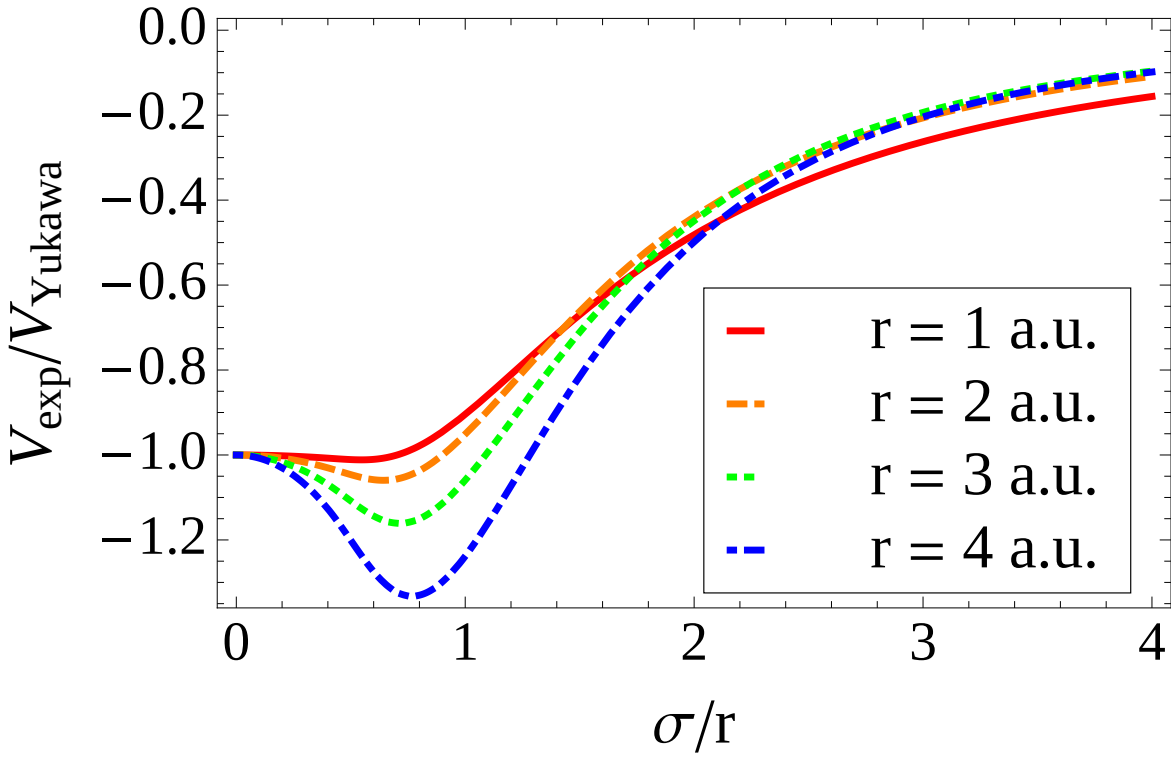

Figure 4. (Color online) The dynamics of the Gaussian WP width σ is governed by the σ dependence of the expectation value of the potential energy between a Gaussian WP electron and a Yukawa screened ion. The graphs show the ratio $V_{exp}(r,\sigma)/V_{\text{Yukawa}}(r)$ between the potential expectation value and the Yukawa potential itself as a function of the ratio between WP width, σ, and the distance between the ion and electron, r. Curves for four different values of r are shown: 1 a.u. (solid red), 2 a.u. (dashed orange), 3 a.u. (dotted green), and 4 a.u. (dot-dashed blue). Note that the minimum in the expection value of the potential is at nonzero values of σ/r unlike for the bare Coulomb potential (similar to the solid red curve). The minimum at nonzero width makes the WP spread towards the distant ions.

protons.

The potential expectation value $V_{exp}(r,\sigma)$ also has a finite asymptote at infinite σ. This asymptote is energetically accessible during the evolution of a WP with a positive energy expectation value. If a WP obtains a large width asymptote, the absence of interaction inhibits a return to small σ.

We expect the exact solution to have a component of its probability current to be directed towards each ion, instead of spreading in all directions. For an isotropic system, this has

little effect on the uncertainty in the position of the electron compared to the Gaussian WP method, but there is a large difference in how much the density will vary as a result. At lower energies, the SOFT wave function visibly localizes near ion clusters in the unit cell, leading to the breakup of the electron density into localized components. Using a single Gaussian WP to represent the wave function fails to capture this breakup, crucial to reproducing the electron density predicted by SOFT. This same breakup also happens for the higher energy cases but to a lesser extent and more visibly at later times than shown in Figs. 2 and 3. We quantify this effect in the following subsection.

D. Quantification of spreading, breakup, and localization

We show the widths predicted by three methods, SOFT, Gaussian WP, and the non-interacting WP in Fig. 5 as defined in the x-direction by

$$\sigma_x = \sqrt{\langle \hat{x}^2 \rangle - \langle \hat{x} \rangle^2} \tag{44}$$

and similarly in the y- and z-directions. Technically, the SOFT wave function is periodic, so the expectation values of moments of position are ill-defined. However, over this short evolution time, the wave function does not spread enough to significantly interfere with itself, so we calculate the expectation values as if the particle is in a non-periodic box centered at the position of the Gaussian WP. The widths grow at roughly the same rate regardless of energy with a slight trend of growing more slowly at higher energies. The growth is lower in the direction of motion because scattering by the nuclei tends to only increase the width in directions orthogonal to the motion. The Gaussian WP gives a reasonable prediction of the mean spreading in the three directions and in all cases has greater width than the non-interacting WP. If anything, the Gaussian WP width is a bit small compared to the SOFT WP, so restricting the growth of the Gaussian WP width [22–29] is unphysical.

The main failure of the Gaussian WP is its inability to represent breakup. In order to quantify the breakup of the WP, we counted the number of local maxima, N_m, in the three dimensional density. A grid point in the SOFT density is a local maximum if it is greater than its 26 nearest neighbors. Many of these are very small in amplitude, so we applied a smoothing filter multiple times. Each application of the filter replaced the density at the grid point by the value midway between the current value and the mean of the 26 nearest

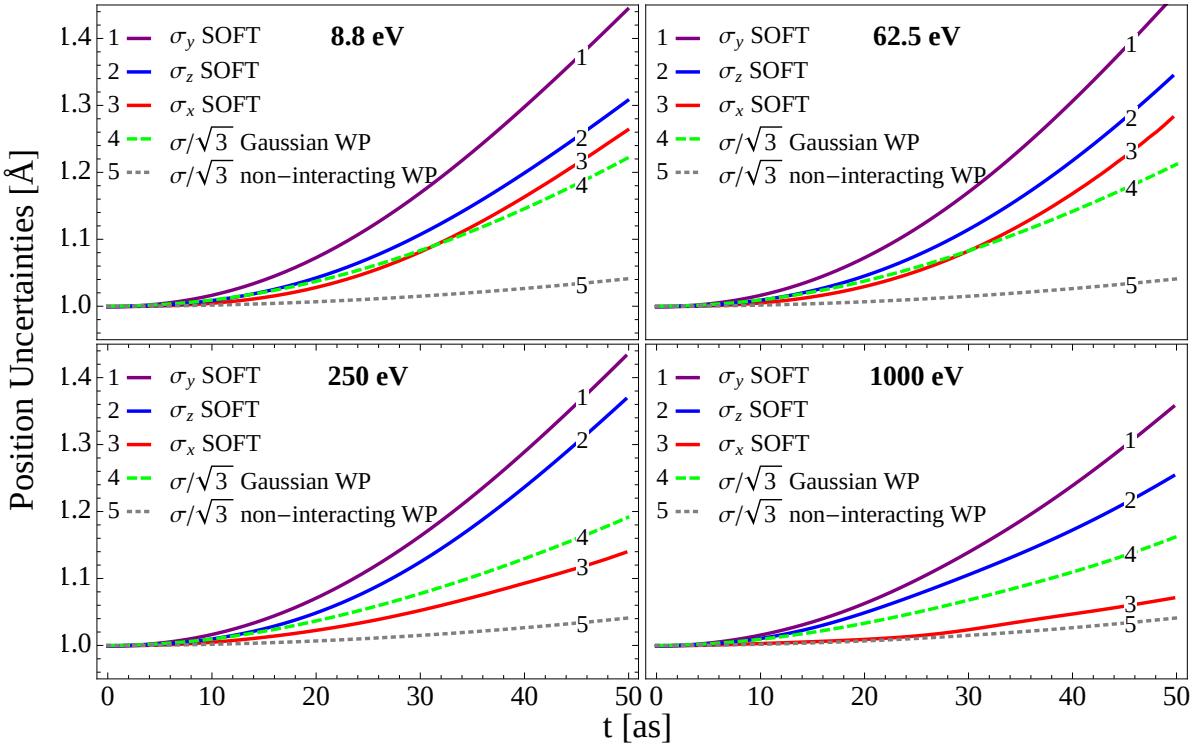

Figure 5. (Color online) The position uncertainties of the SOFT solution in the x- (3, solid red), y- (1, solid purple), and z-directions (2, solid blue), the Gaussian WP (4, dashed green), and non-interacting WP (5, dotted gray) for four different initial values of the translational kinetic energy. The Gaussian WP and non-interacting WP are spherically symmetric, so their positition uncertainties in all three directions are the same.

neighbors. These results are shown in Fig. 6. At first we were surprised that the number quickly grew into the thousands, but detailed inspection reveals that these are actually caused by the interference of all the spherical waves emanating from the scattering centers. In fact, a rough estimate for N_m at large times can be calculated by taking the maximum of the number of cubic de Broglie wavelengths that fit in the box and the number of protons, N_p,

$$N_m(t=\infty) \approx \max\left(N_p, \left(\frac{L}{\Lambda}\right)^3\right), \tag{45}$$

where $\Lambda = h/p$ is the de Broglie wavelength corresponding to the magnitude of the expectation value of the momentum and h is Planck's constant. Equation (45) implies that the lowest two energies produce roughly the same number of maxima, N_p. Their respective WPs

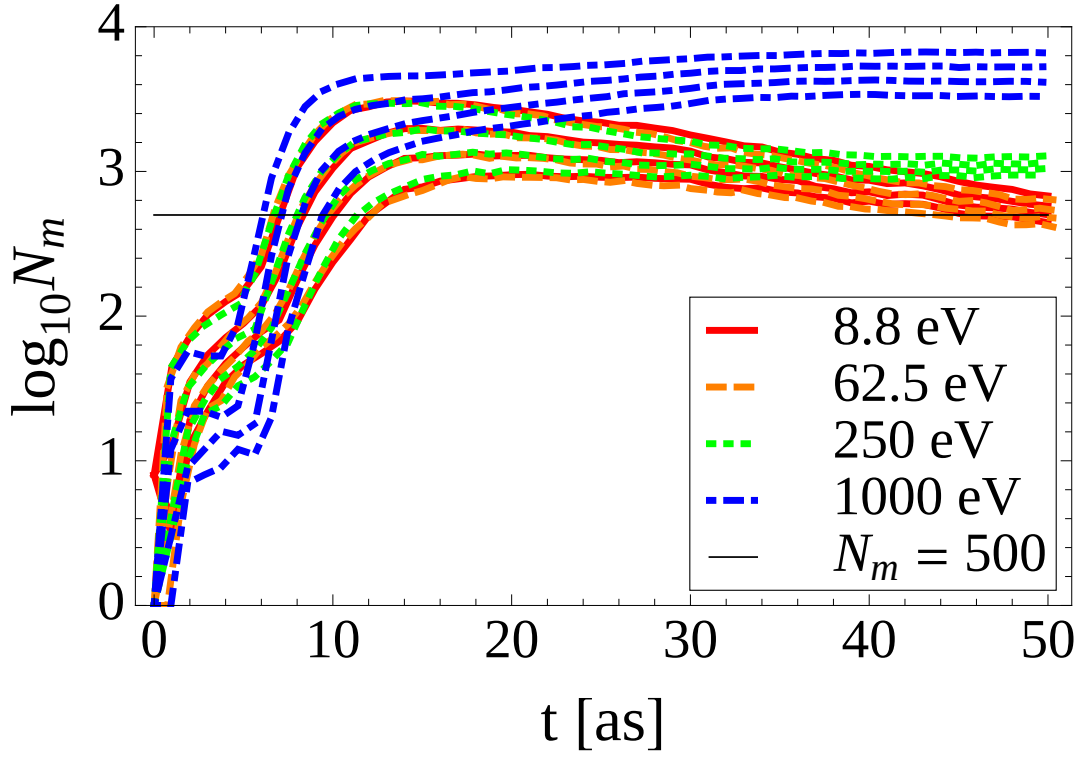

Figure 6. (Color online) The number of local maxima in the SOFT electron density as a function of time for four different WP energies: 8.8 (solid red), 62.5 (dashed orange), 250 (dotted green), and 1000 eV (dot-dashed blue). The lowest two energy cases are nearly indistinguishable. Four curves are shown for each energy representing the number of maxima after zero, one, two, and three passes of a smoothing filter as described in the text. The horizontal line indicates the number of ions in the periodic unit cell. Surpassing this number is indicative of the onset of interference effects.

breakup to produce higher densities near each proton as their bound parts of their densities tunnel to each minimum in the potential and the free parts have greater time averaged densities there. The dynamics of the higher two energies are dominated by continuous free-free scattering and interference between all of the resulting modes. We also note that the highest energy WP is able to remain close to a Gaussian shape for longer, so that at short times there are fewer maxima as shown by Fig. 6.

Another measure of localization is the participation function (PF) [50], defined as the inverse of the integral of the probability density squared,

$$P[\varphi] = \left(\int |\varphi|^4 d\boldsymbol{x} \right)^{-1}. \tag{46}$$

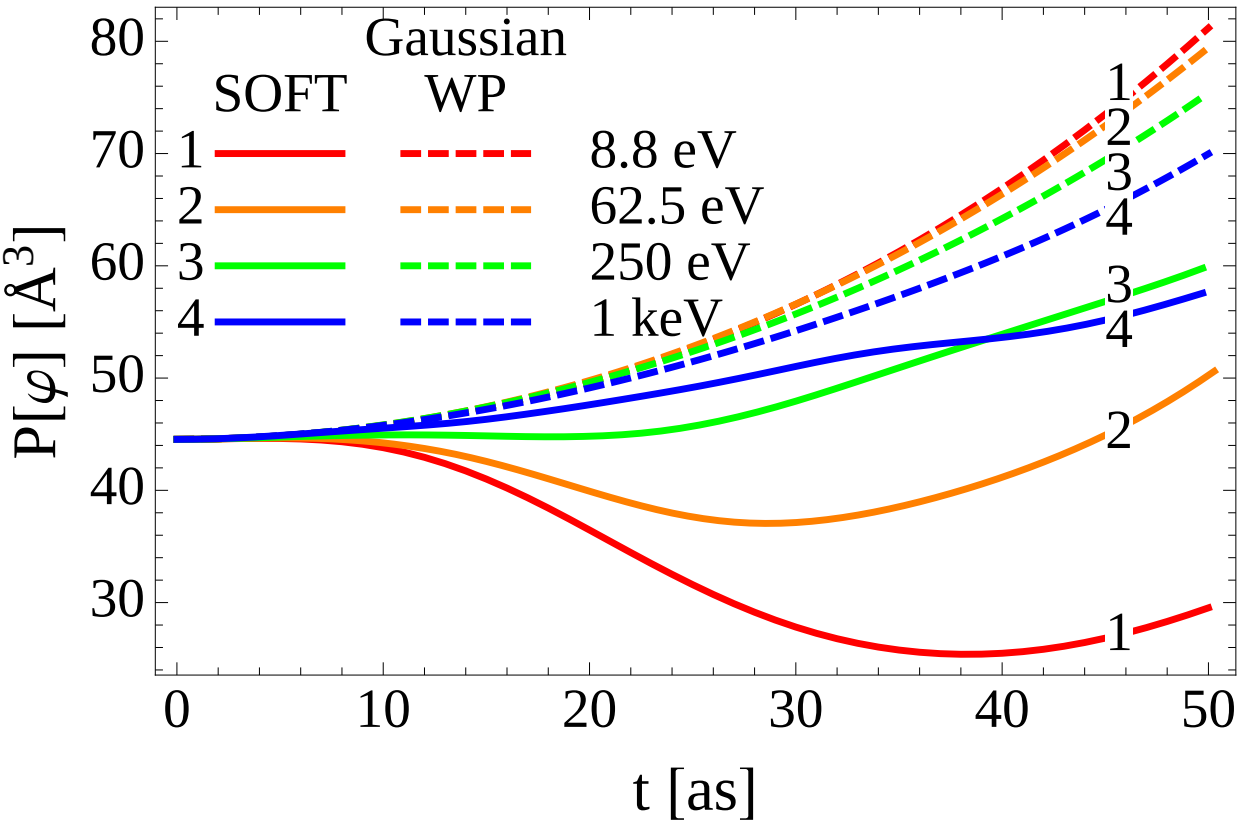

Figure 7. (Color online) The participation function evaluated with the SOFT (solid curves) and Gaussian WP (dashed curves) density for four different values of the initial translational kinetic energy: 8.8 eV (1, red), 62.5 eV (2, orange), 250 eV (3, green), 1000 eV (4, blue).

The PF is a rough measure of the volume occupied by the WP. The two extremes of the PF are the Dirac delta function ($P = 0$) and constant density ($P = L^3$). We have plotted the PF in Fig. 7. Completely different predictions are obtained by Gaussian WP and SOFT. The PFs of SOFT are lower because SOFT properly handles the breakup of the WP, localizing densities to near ions, while in the Gaussian WP simulation the WP spreads by roughly the same amount as the SOFT WP, as shown in Fig. 5, but occupies the entire space inside that width. The two predictions only converge to one another at very high energies ($\gtrsim$ 1000 eV).

Unlike the monotonically growing Gaussian WP PFs, the SOFT PF's time evolution can be divided into three regimes. Before about five attoseconds regardless of the energy, the WP spreads slightly, occupying more volume and increasing the PF. This early behavior is equivalent to the non-interacting electron. This is followed by a period ranging from zero to about thirty attoseconds, depending on the energy, over which time the participation

function decreases when the density "falls" into local potential energy minima. Density does not follow where the non-interacting particle is centered, but becomes localized near the protons. The participation function eventually increases again as the collapse of the density into the minima ends and spreading of both the bound and free parts of the density becomes dominant.

E. Accuracy of approximate methods

The lowest impact energy is the most challenging case. Adding more wave packets, as in the split WP method, significantly improves the final density. Localization similar to that predicted by SOFT is obtained, with the caveat that split WP packets are spherical, while the localized components in SOFT are distorted. This is reflected in the overlaps and density overlaps shown in Figs. 8 and 9, respectively. A steady improvement is obtained by increasing the number of WPs in split WP.

Saturation of the convergence with respect to the number of WPs may be explained by our special choice of basis, where only a small number of Gaussians at selected positions was used. For our choice of initial positions of the auxiliary WPs, the electron density near local peaks is represented more accurately than in the rest of the simulation box. We can see that the WP as predicted by SOFT has only broken up into roughly five pieces of significant size (see Figs. 2 and 3) in 50 as, so convergence beyond $M = 5$ is expected to be slow. At later times the WP is likely to breakup even more, for which a greater value of M is needed. In general, it is necessary to have initial basis functions available at space locations other than at local potential minima only. Increasing the basis size for split WP is theoretically expected to produce results converging to the exact solution.

Another feature of the overlap curves is that they fall off over a time scale of roughly 1 a.u. This is not surprising considering all quantities involved (electron mass, kinetic and potential energies of the electron), are about 1 a.u. as well. We also show the WTM result in Figs. 3 and 9.[2] WTM performs surprisingly well, considering the only quantum effect it includes is the initial uncertainty in position and momentum. However, many more parameters ($300,000$ positions and momenta) than for split WP (at most 50) are required,

[2] We do not calculate a regular overlap for Fig. 8 between the WTM and SOFT states because $50,000$ particles does not produce a good resolution in the six-dimensional phase space. Hence, the overlap would have extensive statistical noise.

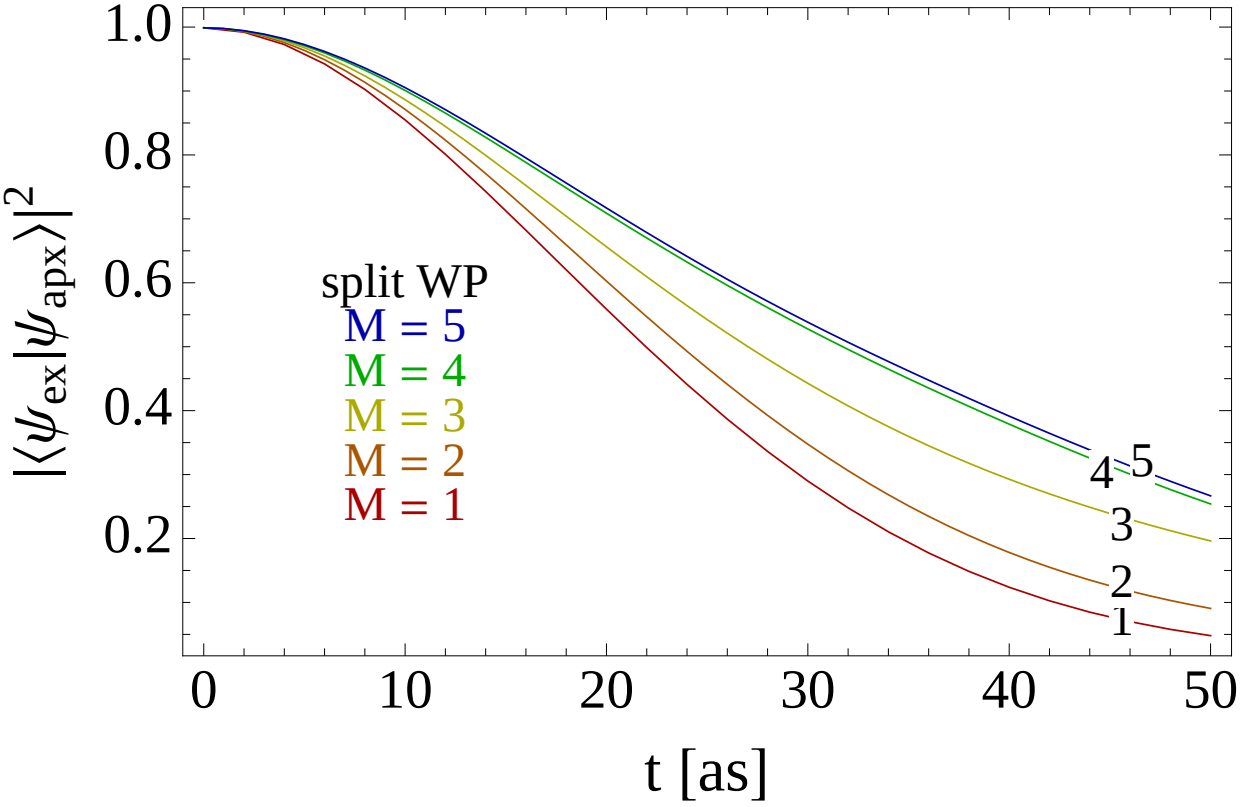

Figure 8. (Color online) Overlaps between the SOFT (ex) and wave functions evolved according to the TDVP as a function of time. Results from one to five WPs indicate systematic improvement from the Gaussian WP ($M = 1$) to split WP ($M = 5$) variational forms. The decay from unity is a consequence of the use of only a small number of Gaussians at selected initial positions. As predicted by SOFT, the initial state breaks up into five pieces of significant size (see Figs. 2 and 3) in 50 as, so convergence beyond $M = 5$ is expected to be slow.

so the greater flexibility in the Wigner function comes at considerable computational cost. Note that, at $t = 0$, the density overlap is not exactly unity due to the statistical sampling of the initial state.

IV. CONCLUSION

We have evolved the state of a single electron in a model plasma with a variety of theoretical methods in order to understand which approximations are valid in the dense plasma regime. We used the TDVP with different variational forms ranging from the single Gaussian WP commonly used in WPMD, up to a sum of five Gaussian WPs (the split WP method).

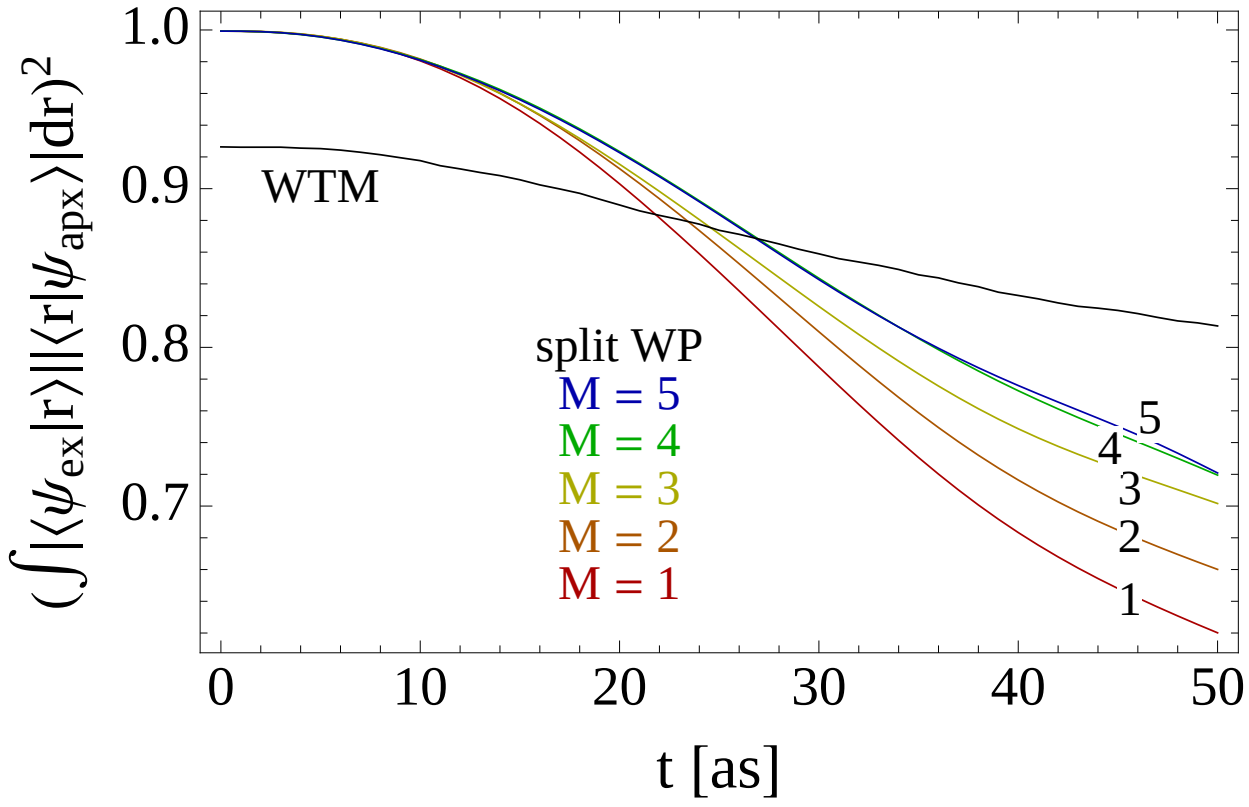

Figure 9. (Color online) Overlap of the spatial densities between those from the SOFT and WTM and the SOFT and split WP methods as a function of time. Initial overlap of WTM and SOFT is not unity due to noise in sampling the initial state.

These were compared with the Thomas-Fermi limit in the WTM, the non-interacting WP, and the numerically exact SOFT solution. We determined what properties are needed in the form of the variational ansatz used by the TDVP and how important the non-locality of quantum mechanics is in predicting the evolution of a WPs density using the WTM.

All of the methods used in this article predict wave packet spreading. The non-interacting WP had the least amount of spreading as measured by the uncertainty in position of the electron. So the use of constraints on the Gaussian WP width to prevent spreading is unphysical and the potential energy increases the rate of spreading. Spreading is the combined result of uncertainty in the WP's momentum, and density accumulating in as many potential energy wells as possible. The former effect is illustrated by the non-interacting WP's evolution in Figs. 2 and 5 and the latter for the simple case of the Gaussian WP by Fig. 4.

The inability of the Gaussian WP to breakup is the main failure of this variational form. The SOFT, WTM, and the split WP methods all predicted breakup of the electron's density

with higher density near the ions. The breakup occurred as the WP spread and was key to properly determine the volume taken up by the density as measured by the participation function (see Fig. 7) at all energies.

Differences in the final density as a function of WP energy were shown in Figs. 2 and 3. We performed the evolution with SOFT, the Gaussian WP, and non-interacting WP with four different values of $\langle \hat{\boldsymbol{p}} \rangle^2/2m$: 8.8, 62.5, 250, and 1000 eV. Different temperature many-body systems would sample these energies differently. Breakup of the WP is most pronounced at lower energies, but is present at all energies because there are always regions near each ion for which the magnitude of the potential energy is greater than the kinetic energy.

Of all the approximate methods, the WTM was best at matching the electron's density, as shown in Figs. 3 and 9, despite completely neglecting all but the first derivatives of the potential energy in Eq. (20) to get Eq. (21). We infer that quantum diffraction and interference are not as important for obtaining the right density as preserving the uncertainty in the position and momentum of the electron. The different parts of the phase space density can then produce approximately the correct spreading and breakup.

The split WP method reproduces breakup as well by allowing that flexibility in the variational ansatz. Convergence was shown towards the SOFT solution in Figs. 8 and 9. However, diminishing returns were seen in adding additional auxiliary WPs. This is especially true when the number of WPs used to create the variational form is greater than the number of regions the exact density has broken into. One is then left with the problem of fitting a function bearing no resemblance to the isotropic Gaussians, especially at large times.

The quantum wave function is the complete description of a quantum state and is therefore challenging to reproduce accurately by approximate methods. Therefore, the temporal drift from the SOFT state of the WTM and split WP results seen in Figs. 8 and 9 is expected. However, these approximations reproduce the breakup of the WPs as shown by Figs. 2 and 3. This indicates that improvements over classical models can be made at the particle level that lead to accurate models for scattering and energy exchange between particles, although such processes have not been studied in this article. In many applications, only the correct dynamics of average properties is needed. Generalizations of the WTM and split WP method to many-body systems are likely to yield improvements over WPMD,

for example, in the averaged screening of ions as expressed by the pair correlation function between electrons and ions.

In considering which method to use for a many-body simulation, it is important to balance computational cost with physical accuracy. The SOFT method is much too expensive to apply to much bigger systems. Table I shows the WTM to be even more expensive for a single particle. However, a sensical generalization of this method to many bodies is to not retain the full $6N$-dimensional Wigner density, but only the total 6-dimensional Wigner density. Such a method would add the complexity of simultaneously solving the Poisson equation to calculate mean field forces and the possible inclusion of a collision term to mimic the effects of the exact particle-particle scattering. This model is kinetic theory molecular dynamics (KTMD) [15].

The split WP method is readily generalized to split WPMD in an exactly analogous way to the generalization of the Gaussian WP method to WPMD. It would be more computationally expensive than WPMD by about the same amount as the split WP is than the Gaussian WP (see Tab. I), which is feasible with modern computers. It is still uncertain how to initialize the quantum state and how to deal with the problem that the exact density will continue to breakup into more and more pieces as time increases.

The failure of the Gaussian WP to allow breakup leads us to reject WPMD as an *ab initio* many-body method for dense plasmas. It can still be treated as an empirical model and as such has had some success (*e.g.* the eFF method), but every new calculation in regimes far from prior successes should be treated with suspicion unless corroborated with experiments and/or other models. None of this work indicates which approximations to the exact Fermi statistics are valid nor whether degeneracy effects alter our conclusions about the validity of WPMD for dense plasmas. At high temperatures ($T \gg T_F$) such effects are irrelevant and WPMD, even fully antisymmetrized would not predict valid electron densities and at lower temperatures the Gaussian shape is too simple to produce proper electron screening or atomic physics.

Acknowledgements

Parts of this work were performed under the auspices of the U.S. Department of Energy by Lawrence Livermore National Laboratory under Contract DE-AC52-07NA27344 and parts

have been authored by employees of the Los Alamos National Security, LLC. (LANS), operator of the Los Alamos National Laboratory under Contract No. DE-AC52-06NA25396 also with the U.S. Department of Energy.

Grabowski, Markmann, Murillo, Fichtl, Richards, Batista, and Graziani are members of the Cimarron collaboration and were funded by the Laboratory Directed Research and Development Program at LLNL under project tracking code 09-SI-011.

Morozov and Valuev acknowledge the support by the Programs of Fundamental Research of RAS Nos. 2, 14 and 15, Russian Foundation for Basic Research (grants 12-02-31783 and 12-02-33170) and Sandia National Laboratories under the U.S. DOE/NNSA Advanced Simulation and Computing program.

We would like to thank James N. Glosli for helpful discussion on implementing WTM.

---

[1] J. Nuckolls, L. Wood, A. Thiessen, and G. Zimmerman, Nature **239**, 139 (1972).

[2] M. D. Knudson, D. L. Hanson, J. E. Bailey, C. A. Hall, J. R. Asay, and C. Deeney, Phys. Rev. B **69**, 144209 (2004).

[3] M. S. Murillo, Phys. Rev. E **81**, 036403 (2010).

[4] R. W. Lee, S. J. Moon, H.-K. Chung, W. Rozmus, H. A. Baldis, G. Gregori, R. C. Cauble, O. L. Landen, J. S. Wark, A. Ng, S. J. Rose, C. L. Lewis, D. Riley, J.-C. Gauthier, and P. Audebert, J. Opt. Soc. Am. B **20**, 770 (2003).

[5] S. H. Glenzer and R. Redmer, Rev. Mod. Phys. **81**, 1625 (2009).

[6] A. W. DeSilva and H.-J. Kunze, Phys. Rev. E **49**, 4448 (1994).

[7] J. F. Benage, W. R. Shanahan, and M. S. Murillo, Phys. Rev. Lett. **83**, 2953 (1999).

[8] S. A. Khairallah and B. Militzer, Phys. Rev. Lett. **101**, 106407 (2008).

[9] J. J. Fortney, S. H. Glenzer, M. Koenig, B. Militzer, D. Saumon, and D. Valencia, Physics of Plasmas **16**, 041003 (2009).

[10] H. F. Wilson and B. Militzer, Phys. Rev. Lett. **108**, 111101 (2012).

[11] J. Vorberger, I. Tamblyn, B. Militzer, and S. A. Bonev, Phys. Rev. B **75**, 024206 (2007).

[12] H. Wang and M. Thoss, J. Chem. Phys. **119**, 1289 (2003).

[13] U. Manthe, J. Chem. Phys. **128** (2008).

[14] C. S. Jones and M. S. Murillo, High Energy Density Physics **3**, 379 (2007).

[15] F. R. Graziani, V. S. Batista, L. X. Benedict, J. I. Castor, H. Chen, S. N. Chen, C. A. Fichtl, J. N. Glosli, P. E. Grabowski, A. T. Graf, S. P. Hau-Riege, A. U. Hazi, S. A. Khairallah, L. Krauss, A. B. Langdon, R. A. London, A. Markmann, M. S. Murillo, D. F. Richards, H. A. Scott, R. Shepherd, L. G. Stanton, F. H. Streitz, M. P. Surh, J. C. Weisheit, and H. D. Whitley, High Energy Density Physics **8**, 105 (2012).

[16] L. X. Benedict, M. P. Surh, J. I. Castor, S. A. Khairallah, H. D. Whitley, D. F. Richards, J. N. Glosli, M. S. Murillo, C. R. Scullard, P. E. Grabowski, D. Michta, and F. R. Graziani, Phys. Rev. E **86**, 046406 (2012).

[17] E. J. Heller, J. Chem. Phys. **62**, 1544 (1975).

[18] H. Feldmeier and J. Schnack, Rev. Mod. Phys. **72**, 655 (2000).

[19] H. Feldmeier, Nuclear Physics A **515**, 147 (1990).

[20] D. Klakow, C. Toepffer, and P.-G. Reinhard, J. Chem. Phys. **101**, 10766 (1994).

[21] D. Klakow, C. Toepffer, and P.-G. Reinhard, Physics Letters A **192**, 55 (1994).

[22] M. Knaup, P.-G. Reinhard, and C. Toepffer, Contributions to Plasma Physics **39**, 57 (1999).

[23] M. Knaup, G. Zwicknagel, P. G. Reinhard, and C. Toepffer, J. Phys. IV France **10**, 307 (2000).

[24] M. Knaup, G. Zwicknagel, P. G. Reinhard, and C. Toepffer, Nuclear Instruments and Methods in Physics Research Section A: Accelerators, Spectrometers, Detectors and Associated Equipment **464**, 267 (2001).

[25] M. Knaup, P.-G. Reinhard, and C. Toepffer, Contributions to Plasma Physics **41**, 159 (2001).

[26] M. Knaup, P.-G. Reinhard, C. Toepffer, and G. Zwicknagel, Computer Physics Communications **147**, 202 (2002), proceedings of the Europhysics Conference on Computational Physics Computational Modeling and Simulation of Complex Systems.

[27] M. Knaup, P.-G. Reinhard, C. Toepffer, and G. Zwicknagel, Journal of Physics A: Mathematical and General **36**, 6165 (2003).

[28] W. Ebeling, A. Filinov, M. Bonitz, V. Filinov, and T. Pohl, Journal of Physics A: Mathematical and General **39**, 4309 (2006).

[29] I. V. Morozov and I. A. Valuev, Journal of Physics A: Mathematical and Theoretical **42**, 214044 (2009).

[30] J. T. Su and W. A. Goddard, Phys. Rev. Lett. **99**, 185003 (2007).

[31] A. Lenglet, G. Maynard, and Y. K. Kurilenkov, Journal of Physics A: Mathematical and

General **39**, 4671 (2006).

[32] B. Jakob, P.-G. Reinhard, C. Toepffer, and G. Zwicknagel, Phys. Rev. E **76**, 036406 (2007).

[33] B. Jakob, P.-G. Reinhard, C. Toepffer, and G. Zwicknagel, Journal of Physics A: Mathematical and Theoretical **42**, 214055 (2009).

[34] J. T. Su and W. A. Goddard, Journal of Chemical Physics **131**, 244501 (2009).

[35] A. Jaramillo-Botero, J. Su, A. Qi, and W. A. Goddard, Journal of Computational Chemistry **32**, 497 (2011).

[36] G. V. Boriskov, A. I. Bykov, R. I. Il'kaev, V. D. Selemir, G. V. Simakov, R. F. Trunin, V. D. Urlin, A. N. Shuikin, and W. J. Nellis, Phys. Rev. B **71**, 092104 (2005).

[37] A. K. Kerman and S. E. Koonin, Annals of Physics **100**, 332 (1976).

[38] I. V. Morozov and I. A. Valuev, Contributions to Plasma Physics **52**, 140 (2012).

[39] H.-W. Lee and M. O. Scully, The Journal of Chemical Physics **73**, 2238 (1980).

[40] C.-Y. Wong, Phys. Rev. C **25**, 1460 (1982).

[41] H.-W. Lee and M. O. Scully, Foundations of Physics **13**, 61 (1983).

[42] E. Wigner, Phys. Rev. **40**, 949 (1932).

[43] M. P. Allen and D. J. Tildesley, Computer Simulation of Liquids (Oxford Science Publications, Oxford, 1987).

[44] A. Markmann, F. Graziani, and V. S. Batista, Journal of Chemical Theory and Computation **8**, 24 (2012).

[45] M. D. Feit and J. J. A. Fleck, J. Chem. Phys. **78**, 301 (1983).

[46] M. D. Feit and J. J. A. Fleck, J. Chem. Phys. **80**, 2578 (1984).

[47] A. D. Bandrauk and H. Shen, J. Chem Phys. **99**, 1185 (1993).

[48] N. Balakrishnan, C. Kalyanaraman, and N. Sathyamurthy, Phys. Rep. **280**, 80 (1997).

[49] C. Leforestier, R. H. Bisseling, C. Cerjan, M. D. Feit, R. Friesner, A. Guldberg, A. Hammerich, G. Jolicard, W. Karrlein, H.-D. Meyer, N. Nipkin, O. Roncero, and R. Kosloff, J. Comp. Phys. **94**, 59 (1991).

[50] F. Wegner, Z Phys B **36**, 209 (1980).